

# Methanol Adsorption and Reactivity on Clean and Hydroxylated Anatase(101) Surfaces

Antonio Tilocca\* and Annabella Selloni

Department of Chemistry, Princeton University, Princeton, New Jersey 08540

Received: August 7, 2004; In Final Form: September 11, 2004

The adsorption and reactivity of methanol on TiO<sub>2</sub> anatase(101) surfaces are studied through first-principles total energy calculations and Car–Parrinello molecular dynamics simulations. The effects of different methanol coverages up to one monolayer and different surface oxidation states are investigated. The most stable monolayer state involves two different molecular adsorption states, with specific vibrational and electronic properties. Molecular adsorption is always favored on the stoichiometric surface, even though dissociation becomes increasingly more favorable with increasing coverage. Oxygen vacancies shift the energy balance in favor of the dissociated state, whereas dissociative and molecular adsorption appear competitive on the hydroxylated surface. On the latter, a specific molecular adsorption mode, not available on the clean surface, turns out to be stable. The vibrational and electronic properties of adsorbed methanol and methoxy are determined and compared to available experimental data.

## 1. Introduction

Titanium oxide is one of the most studied metal oxides due to its many applications in photocatalysis, solar cells, photoelectrolytic water splitting, sensors, and biomaterials.<sup>1</sup> Extensive research involves the use of TiO<sub>2</sub> as primary photocatalyst for the removal of toxic organic pollutants from air and water.<sup>2</sup> Methanol is a simple prototype for organic compounds: it can be oxidized to formaldehyde by disproportionation of methoxy groups formed upon dissociation or by reaction with adsorbed molecular oxygen.<sup>3</sup> It also represents a suitable molecular probe to explore surface properties through several experimental techniques. Moreover, it has an important role in photocatalysis as a hole scavenger.<sup>4,5</sup> For these reasons methanol chemistry on TiO<sub>2</sub> surfaces has recently received considerable attention.<sup>3,6–8</sup>

On the vacuum annealed rutile TiO<sub>2</sub>(110) surface, temperature programmed desorption (TPD), low energy electron diffraction (LEED), and high resolution electron energy loss spectroscopy (HREELS) measurements have shown that most adsorbed methanol is in the molecular state, with methoxy groups generally associated to vacancy sites; however, at variance with water adsorption on the same surface,<sup>9,10</sup> some evidence of methanol dissociation at nondefect sites also has been reported. In agreement with these experimental results, first-principles periodic calculations<sup>6</sup> have shown that on the nondefective TiO<sub>2</sub>(110) surface the energies of molecular and dissociative states lie within a narrow range for half-layer (HL) and monolayer (ML) adsorption.

The situation is somewhat more confused for the more photocatalytically active anatase surface.<sup>11</sup> Single-crystal X-ray photoelectron spectroscopy (XPS) data have shown no evidence of methanol dissociation, whereas features of methoxy groups were detected by TPD on the same sample and attributed to CH<sub>3</sub>OH dissociation at step edges.<sup>7</sup> Similarly, sum-frequency generation (SFG) experiments on a nanoparticulate anatase film<sup>8</sup> have found that molecular adsorption dominates at nonvacancy sites, whereas chemisorption with methoxy formation is related to defects. At variance with ref 7, however, in the latter study,

methanol dissociation has been attributed to reaction with surface bridging hydroxyls, which in turn are formed by H<sub>2</sub>O dissociation at oxygen vacancies. The latter process is enhanced by UV irradiation, thus explaining the increase in the methoxy signal after UV pretreatment of the anatase sample.

The purpose of this paper is to provide further insight into the structure of methanol on anatase surfaces, by presenting the results of first-principles total energy and molecular dynamics calculations for methanol adsorption on clean, hydroxylated, and partially reduced anatase(101) surfaces. Molecular dynamics (MD) simulations have been performed to efficiently sample the configuration space and to identify the most stable equilibrium structures. MD trajectories were also used to calculate vibrational spectra and to check the stability of selected structures.

We provide evidence that molecular adsorption is always favored on the stoichiometric clean surface, although the dissociation probability increases with coverage. The main adsorption modes and energetics are similar to H<sub>2</sub>O adsorption on the same surface, in agreement with their similar TPD spectra.<sup>7</sup> Differences in the structure of an adsorbed monolayer compared to water are determined by significant repulsion between methyl groups. On the partially hydroxylated surface, a new molecular adsorption mode is found, which is roughly isoenergetic with the dissociated state formed by reaction with a surface OH. On the other hand, direct dissociation at an oxygen vacancy shows a very favorable energy balance.

## 2. Computational Methods

Geometry optimizations and molecular dynamics simulations have been performed within the Car–Parrinello<sup>12</sup> approach, using the PBE exchange–correlation functional<sup>13</sup> and ultrasoft pseudopotentials<sup>14</sup> including C and O 2s, 2p and Ti 3s, 3p, 3d, 4s shells. Plane-wave basis set cutoffs for the smooth part of the wave functions and the augmented density were 25 and 200 Ry, respectively. *k*-sampling was restricted to the  $\Gamma$  point. The surface was modeled as a periodic slab of four Ti<sub>4</sub>O<sub>8</sub> layers (6 Å thick) with a surface area of 10.24 × 7.57 Å<sup>2</sup>, corresponding to a 1 × 2 surface unit cell. Four 5-fold-coordinated titanium

\* Corresponding author. E-mail: atilocca@princeton.edu.

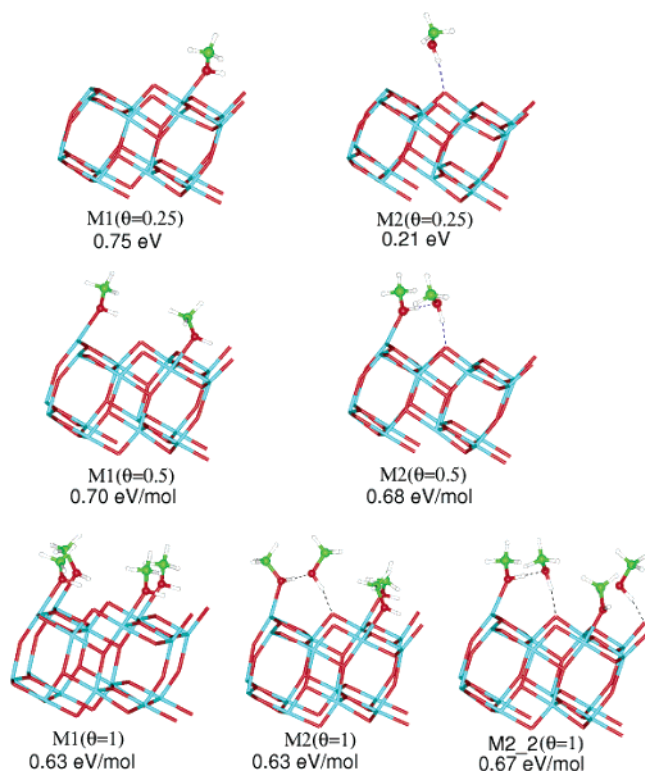


**Figure 1.** Optimized adsorption structures and energies of molecular methanol at different coverages on the defect-free surface.

atoms (Ti<sub>5c</sub>) are the main adsorption sites exposed in this cell. 3D periodic boundary conditions were applied, with a  $\sim 10$  Å vacuum layer along  $z$ . The atoms in the bottom layer were always fixed to their bulk positions. The defective surface was modeled by removing a surface bridging oxygen from a larger ( $10.24 \times 11.36$  Å<sup>2</sup>)  $1 \times 3$  surface cell. All these approximations were extensively tested in our previous studies of TiO<sub>2</sub> systems.<sup>15–19</sup> Geometry optimizations were carried out through damped molecular dynamics until the largest component in the forces on all mobile ions was less than 0.05 eV/Å. In the molecular dynamics runs, a time step of 0.145 fs and a fictitious electronic mass of 700 atomic units were used, together with a 2 amu hydrogen mass. Ionic temperature was controlled by means of a Nosé thermostat.<sup>20</sup>

### 3. Methanol Adsorption on Clean (101) Surfaces

**3.1. Molecular Adsorption.** On the defect-free, stoichiometric (101) surface we investigated a variety of molecular structures with coverages ranging from  $\theta = 0.25$  to 1 ML, see Figure 1. At low coverage ( $\theta = 0.25$ ), methanol adsorption shows features similar to those previously found for water on the same anatase(101) surface.<sup>16,18,19</sup> Molecular adsorption is favored: in the most stable structure (M1), the CH<sub>3</sub>OH molecule is coordinated to a surface Ti<sub>5c</sub> with an adsorption energy of 0.75 eV, very close to that found for a single water molecule.<sup>16</sup> In this coordination mode, the hydroxyl hydrogen points toward a 2-fold-coordinated bridging oxygen (O<sub>2c</sub>) and the methyl group points upward, in a way analogous to molecular CH<sub>3</sub>OH adsorption on rutile(110).<sup>6</sup> Another relevant molecular adsorption structure, denoted as M2( $\theta=0.25$ ), involves the coordination to an O<sub>2c</sub> through hydrogen bond (Hb) donation from the hydroxyl. This CH<sub>3</sub>OH–O<sub>2c</sub> coordination is much less stable than CH<sub>3</sub>OH–Ti<sub>5c</sub> in the M1 configuration; however, a second CH<sub>3</sub>OH adsorbed on an adjacent Ti<sub>5c</sub> (structure M2 at  $\theta = 0.5$ ) stabilizes it considerably through H-bonding: the adsorption

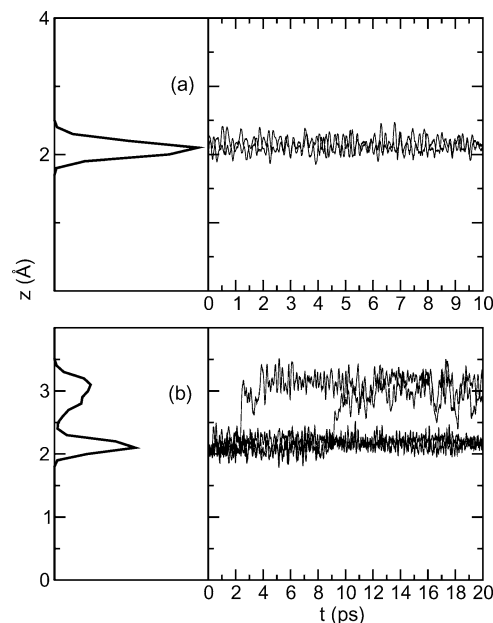


**Figure 2.** Time evolution of the perpendicular distance  $z$  from the surface of the methanol O atoms (right panels) and corresponding distribution (left panels) for (a) two (half-layer) and (b) four (monolayer) methanol molecules on the defect-free surface.

energy increases from 0.21 eV for M2( $\theta=0.25$ ) to 0.68 eV per molecule for M2( $\theta=0.5$ ). This stabilization of CH<sub>3</sub>OH–O<sub>2c</sub> coordination by hydrogen bonds with CH<sub>3</sub>OH–Ti<sub>5c</sub> molecules is similar to that found for H<sub>2</sub>O–O<sub>2c</sub> on the same surface.<sup>19</sup>

To investigate the adsorption of methanol at half-layer (HL) and monolayer (ML) coverage, two and four methanol molecules were initially arranged on the four Ti<sub>5c</sub> present in our simulation cell, respectively. Relatively long MD simulations were carried out to allow the system to efficiently explore the configuration space and find the most stable minima. The system was equilibrated at 160 K for 1–2 ps, followed by a production run of 10 (HL) and 20 ps (ML). The simulation temperature was rather low to prevent CH<sub>3</sub>OH desorption from the surface: TPD results indicate CH<sub>3</sub>OH–O<sub>2c</sub> desorption above 170 K.<sup>7</sup> In the HL case, the two molecules remained bonded to the Ti<sub>5c</sub> during the whole MD run, as shown by the time dependence of the perpendicular distance,  $z(t)$ , of methanol O atoms from the surface (Figure 2a). Thus the corresponding height distribution has a single sharp peak centered at 2.1 Å above the surface. By contrast, the initial configuration with four CH<sub>3</sub>OH–Ti<sub>5c</sub> is not as stable (see Figure 2b): after 3 ps one molecule leaves the CH<sub>3</sub>OH–Ti<sub>5c</sub> layer and moves about 1 Å above, in a coordination similar to M2 in Figure 1. This CH<sub>3</sub>OH–Ti<sub>5c</sub> → CH<sub>3</sub>OH–O<sub>2c</sub> shift is followed by a second one 7 ps later. The resulting configuration, with two CH<sub>3</sub>OH–Ti<sub>5c</sub> and two CH<sub>3</sub>OH–O<sub>2c</sub> remains stable in the following 10 ps at 160 K (Figure 2b). Two peaks are thus present in the  $z(t)$  distribution; the peak at higher  $z$  is broader, due to the larger  $z(t)$  oscillations of CH<sub>3</sub>OH–O<sub>2c</sub> molecules. At variance with water adsorption, where an ordered monolayer of H<sub>2</sub>O–Ti<sub>5c</sub> appears to be very stable,<sup>21</sup> the bulkier CH<sub>3</sub>OH molecules do not form a flat monolayer, but are arranged in a bilayerlike structure already at ML coverage, with half CH<sub>3</sub>OH coordinated to Ti<sub>5c</sub> and the other half coordinated to O<sub>2c</sub>. No CH<sub>3</sub>OH dissociation was observed along the MD trajectories for both HL and ML coverage on the perfect surface.

Relative to the most stable low-coverage M1( $\theta=0.25$ ) structure, the adsorption energy per molecule at the Ti<sub>5c</sub> sites decreases by 0.05 eV/mol at HL coverage (M1( $\theta=0.5$ )), and

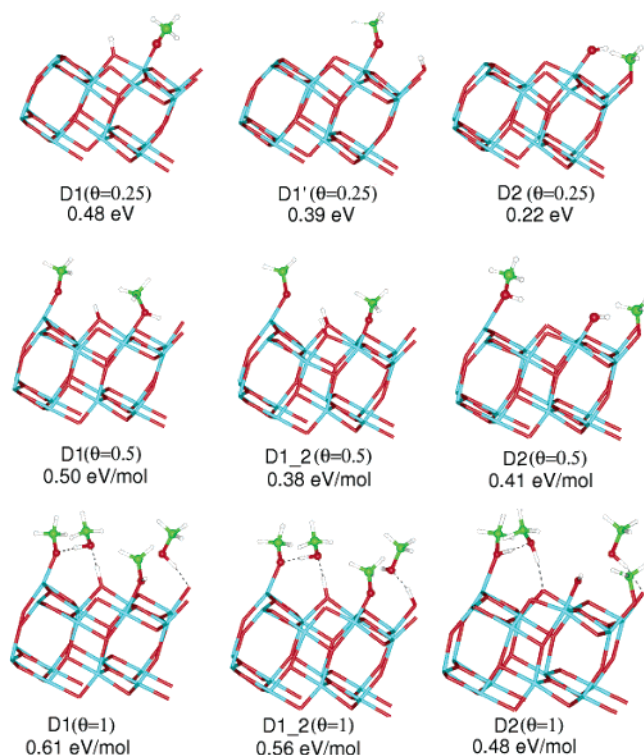


**Figure 3.** Optimized adsorption structures and energies for dissociated methanol at different coverages on the defect-free surface.

by 0.12 eV/mol at ML coverage ( $M1(\theta=1)$ ). More favorable adsorption energies at half-coverage vs full coverage were also found for  $CH_3OH$  on rutile(110).<sup>6</sup> In our case, the most stable ML structure is obtained by shifting two  $CH_3OH-Ti_{5c}$  to  $CH_3OH-O_{2c}$  ( $M2\_2(\theta=1)$ ), as suggested by the MD simulation. The TPD spectra for  $CH_3OH$  on anatase<sup>7</sup> show a peak corresponding to  $CH_3OH-O_{2c}$  between 0.75 and 1.2 ML, indicating  $CH_3OH-O_{2c}$  coordination before ML saturation, in agreement with our results.

The main message emerging from the results of this section is that interactions between adsorbed molecules at higher coverages tend to destabilize  $CH_3OH-Ti_{5c}$  coordination in favor of either  $CH_3OH-O_{2c}$  coordination or dissociation (see below).

**3.2. Dissociative Adsorption.** **3.2.1. Low Coverage.** Turning to dissociative adsorption, two kinds of dissociations are in principle possible: one involving O–H and the other involving C–O breaking. The O–H bond in gas-phase methanol is stronger than C–O,<sup>22,23</sup> so that C–O dissociation would in principle be possible. On rutile(110),  $CH_3OH$  dissociation through both C–O and O–H scission was reported to be thermodynamically possible, but only the latter was actually observed in a MD run, indicating the presence of some kinetic barrier for C–O breaking.<sup>6</sup> On the stoichiometric anatase surface, we find that at low coverage O–H scission is also thermodynamically more favorable. Starting from  $M1(\theta=0.25)$  in Figure 1, structure  $D2(\theta=0.25)$  in Figure 3 is ideally the product of C–O breaking; its adsorption energy is only 0.22 eV, considerably lower with respect to the structures D1 and D1' that result from O–H bond breaking. The latter two structures differ by the location of the transferred proton: in D1 (more stable), the proton is transferred to an  $O_{2c}$  directly linked to the same  $Ti_{5c}$  where the molecule is adsorbed, whereas in D1' it is transferred to the next nearest  $O_{2c}$ .

In any case, molecular adsorption is more favorable at low coverage. As previously found for water,<sup>9,18,19,24</sup> the low stability of dissociated structures on the perfect surface may be

related to the formation of unstable “terminal” hydroxyl ( $OH_t$ ) or methoxy ( $CH_3O_t$ ) groups. The relative stability of dissociated structures seems to indicate that terminal hydroxyls (present in D2) are less stable than terminal methoxy groups (present in both D1 and D1'), or alternatively that bridging methoxy groups are less stable than bridging hydroxyls.

**3.2.2. Half-Layer and Monolayer Coverage.** On rutile(110), Bates et al.<sup>6</sup> found that  $CH_3OH$  dissociation is slightly favored over molecular adsorption at HL coverage, whereas the stability of these two configurations is approximately the same at ML coverage. However, only one  $CH_3OH$  molecule was included in the calculations of ref 6, thus excluding the possibility of a mixed molecular-dissociative ML structure, as found for water on perfect  $TiO_2$  rutile.<sup>25</sup>

On the defect-free anatase(101) surface, we considered several HL and ML structures with partially as well as fully dissociated  $CH_3OH$  layers. Only the dissociation of  $CH_3OH-Ti_{5c}$  molecules was examined, although the process may involve  $CH_3OH-O_{2c}$  as well (see below). In the HL case, the “mixed” state D1- ( $\theta=0.5$ ) shown in Figure 3 is more stable than the fully dissociated D1\_2( $\theta=0.5$ ), but they are both less stable than the molecular state  $M1(\theta=0.5)$  (Figure 1). As in the low-coverage case, C–O breaking, forming D2( $\theta=0.5$ ), is thermodynamically less favored than O–H breaking, which leads to D1( $\theta=0.5$ ).

At monolayer coverage, partially dissociated states become relatively more stable than at low  $\theta$ . Starting from the most stable molecular structure  $M2\_2(\theta=1)$  in Figure 1, the dissociation of either one (D1 and D2) or both (D1\_2)  $CH_3OH-Ti_{5c}$  molecules was considered. The adsorption energy of D1( $\theta=1$ ) is only slightly lower than that of the initial molecular state  $M2\_2$ , and comparable to the other molecular states M1 and M2 at  $\theta=1$ . The relative stability of D1 and D2 confirms that methanol dissociation through C–O bond breaking is less favored than that through O–H breaking. Structure D1\_2( $\theta=1$ ), with both  $CH_3OH-Ti_{5c}$  dissociated, is less stable. It is interesting to note that the dissociative process of a  $CH_3OH-Ti_{5c}$  may involve a  $CH_3OH-O_{2c}$ , which accepts and then transfers a proton to the  $O_{2c}$  to which it is linked by hydrogen bond. We have previously observed a similar mechanism for water dissociation at 2 ML coverage on a defective anatase(101) surface.<sup>19</sup> We checked the stability of structure D1( $\theta=1$ ) by running a short (2 ps) MD trajectory. After 0.3 ps a recombination to molecular methanol (structure  $M2\_2(\theta=1)$ ) took place, again with the participation of a  $CH_3OH-O_{2c}$ , which extracts a proton from  $O_{2c}$ , forming a very short-lived  $CH_3OH_2^+$  species, which immediately transfers a proton back to the neighbor  $Ti_{5c}$ -methoxy group.

Altogether, the results so far reported suggest that intermolecular  $CH_3OH-CH_3OH$  interactions are generally less favorable for molecular than for dissociative adsorption, thus resulting in an enhancement of the dissociation probability with increasing coverage. Despite this effect,  $CH_3OH$  dissociation does not seem likely to occur on the stoichiometric anatase(101) surface up to ML coverage.

**3.2.3. Defective Surface.** Oxygen vacancies are less common in anatase compared to rutile, due to the higher undercoordination of Ti atoms formed upon removal of a bridging oxygen.<sup>7</sup> This low coordination, however, makes the vacancy sites very reactive,<sup>18</sup> and the possibility of a direct  $CH_3OH$  dissociation at a vacancy should be taken into account.

The thermodynamics of  $CH_3OH$  dissociation at an  $O_{2c}$  vacancy shows that the process is indeed very favorable. The adsorption energy of molecular  $CH_3OH$  adsorbed on a 4-fold coordinated Ti ( $M1_v$  in Figure 4) is 1.29 eV; this state is 0.3



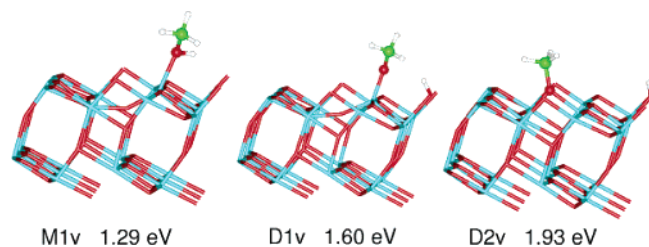


**Figure 4.** Optimized adsorption structures and energies for a methanol molecule on the defective surface.

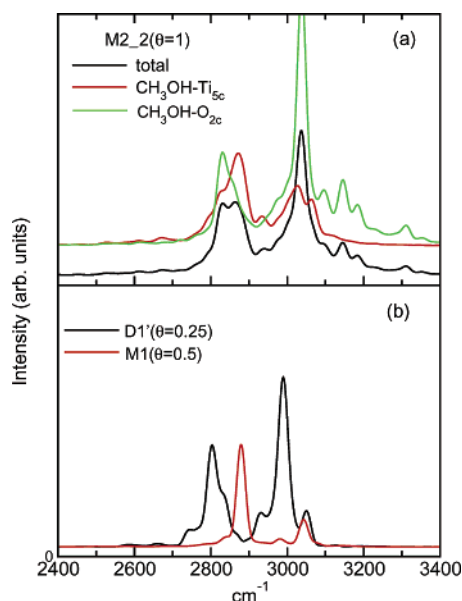


**Figure 5.** Vibrational spectra calculated as Fourier transforms of velocity autocorrelation functions. (Top panel) Monolayer coverage: total spectrum (black); CH<sub>3</sub>OH-Ti<sub>5c</sub> and CH<sub>3</sub>OH-O<sub>2c</sub> contributions (red and green, respectively). (Bottom panel) Molecular CH<sub>3</sub>OH (red) and OCH<sub>3</sub> (black) vibrational spectra. Frequencies have been rescaled by  $\sqrt{2}$  to correct for the 2 amu hydrogen mass used in the MD simulations.

eV less stable than the dissociated state obtained by moving the OH proton to an O<sub>2c</sub> (D1v in Figure 4). This is at variance with H<sub>2</sub>O dissociation, where the first dissociation step is thermoneutral, and the driving force of the reaction is the subsequent migration of a terminal hydroxyl to fill the vacancy.<sup>18</sup> This difference reflects again the higher stability of terminal methoxy groups with respect to terminal hydroxyls. However, as for water, the final state for CH<sub>3</sub>OH dissociation at a vacancy involves a bridging methoxy group, leading to a further energy gain of 0.33 eV (D2v in Figure 4). Overall, the energy balance of vacancy-induced dissociation is more favorable for methanol (0.64 eV) than water (0.37 eV).<sup>18</sup> It is interesting to remark that methanol dissociation by C-O bond breaking would lead to the same final state D2v, after migration of the terminal hydroxyl to the vacancy.

**3.3. Vibrational and Electronic Properties.** The vibrational spectra of adsorbed methanol and methoxy have been calculated by Fourier transforming the velocity autocorrelation functions calculated from MD trajectories. Figure 5a shows the high-frequency region of the methanol ML spectrum for the most stable monolayer structure M2\_2. The symmetric and antisymmetric CH<sub>3</sub> stretching bands are centered at 2852 and 3038 cm<sup>-1</sup>, respectively, to be compared with experimental values of 2855 and 2968 cm<sup>-1</sup>.<sup>26</sup> The first band is split into two peaks, at 2832 and 2865 cm<sup>-1</sup>: this splitting arises from the presence of two CH<sub>3</sub>OH molecules with different coordination in M2\_2,

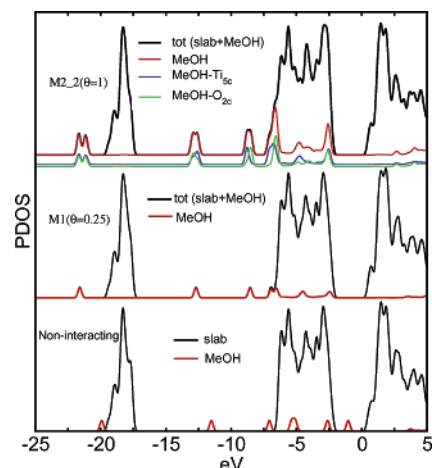


**Figure 6.** Total and projected electronic density of states for CH<sub>3</sub>OH adsorption on the stoichiometric surface. The curves are aligned by matching a semicore Ti state in the bottom layer of the slab. Bottom: noninteracting subsystems; the total DOS is projected onto slab atoms (black curve) and onto methanol atoms (red). Middle: structure M1 ( $\theta = 0.25$ ); total DOS is black, PDOS onto methanol is red. Top: structure M2\_2 ( $\theta = 1$ ); total DOS is black, PDOS onto methanol is red, PDOS onto CH<sub>3</sub>OH-Ti<sub>5c</sub> and CH<sub>3</sub>OH-O<sub>2c</sub> are blue and green, respectively.

as shown by the vibrational spectra calculated separately for CH<sub>3</sub>OH-Ti<sub>5c</sub> and CH<sub>3</sub>OH-O<sub>2c</sub>, also reported in Figure 5a.

Figure 5b shows the vibrational spectra for adsorbed CH<sub>3</sub>OH and CH<sub>3</sub>O, calculated from the 160 K MD trajectories of M1- ( $\theta=0.5$ ) and D1' ( $\theta=0.25$ ). In both structures the interaction between adsorbed species is negligible, so that their comparison is useful to highlight the vibrational features of molecular vs dissociated methanol. The most evident feature is the red-shift of CH<sub>3</sub>O bands with respect to molecular CH<sub>3</sub>OH, in agreement with the trend reported in refs 8 and 27 for CH<sub>3</sub>OH adsorbed on TiO<sub>2</sub>. The peaks in the M1 ( $\theta=0.5$ ) vibrational spectrum roughly coincide with the CH<sub>3</sub>OH-Ti<sub>5c</sub> peaks in Figure 5a, although the latter are significantly broadened due to the hydrogen bonds involving every molecule.

We next investigate the electronic structure of adsorbed methanol on the stoichiometric surface, by considering the total density of states (DOS) and its projection onto the atomic orbitals of methanol molecules (PDOS). In the bottom panel of Figure 6 the DOS of the isolated (noninteracting) slab and methanol molecule are plotted. To align the two curves, a CH<sub>3</sub>OH molecule was placed far above the surface, and the total DOS of this noninteracting system was projected onto the slab and methanol subsystems. The DOS calculation also has been performed for the stable M1 ( $\theta=0.25$ ) and M2\_2 ( $\theta=1$ ) configurations; the curves in the top and middle panels of Figure 6 were aligned to the noninteracting DOS by matching the energy of a semicore (3s) level of a Ti atom in the bottom layer (which should not be affected by the presence of the adsorbates). The interaction with the surface shifts the methanol HOMO from well within the anatase band gap to just below the valence band edge. It is interesting to note that for water on the same surface the HOMO of the adsorbed molecule is pushed well below the valence band edge. This feature reflects the hole-scavenger properties of methanol: the overlap between surface hole states generated by photoexcitation and these filled methanol states favors electron transfer to fill the holes. The DOS projected on adsorbed methoxy groups (Figure 7) shows in detail the region near the band gap. It is interesting to observe that for a terminal OCH<sub>3</sub> (D1) the high-energy band is even closer to the VBM

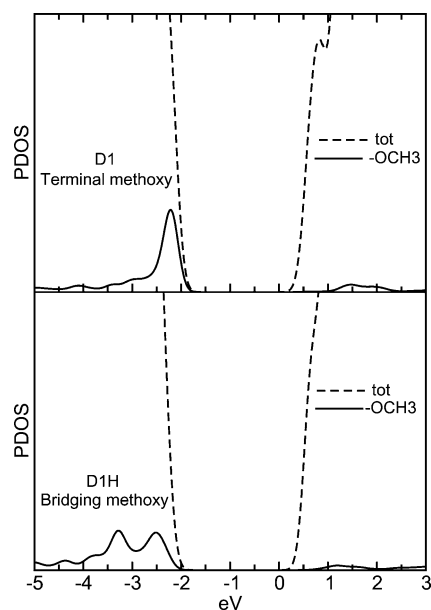
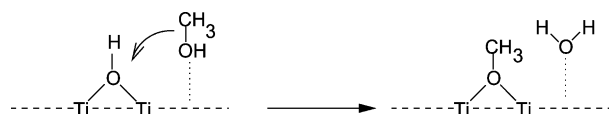


**Figure 7.** PDOS calculated for D1 and D1H structures; only the region near the gap is shown.

#### SCHEME 1: Dissociation at the Hydroxylated Surface



than for a bridging  $\text{OCH}_3$  (D1H), reflecting the higher photoactivity of terminal methoxy groups.<sup>27</sup>

The position of the highest energy band of the methanol PDOS is unchanged at ML coverage. However, the other peaks in the  $\text{CH}_3\text{OH}$  PDOS are significantly modified, compared to lower coverage. The peaks at  $-4.5$ ,  $-12.7$ , and  $-21.5$  eV are split and somewhat broadened. Examining the PDOS projected separately onto  $\text{CH}_3\text{OH}-\text{Ti}_{5c}$  and  $\text{CH}_3\text{OH}-\text{O}_{2c}$  molecules, superimposed in the top panel of Figure 6, one may infer that the different coordination mode determines the splitting of the first two peaks, while the splitting of the peak at lower energy is of different nature. Indeed, this peak corresponds to O 2s orbitals, and the splitting occurs for every  $\text{CH}_3\text{OH}$  molecule, regardless of coordination. The highest energy band in the  $\text{CH}_3\text{OH}$  PDOS mainly involves oxygen p orbitals, while C p orbitals also contribute to the bands between  $-8.7$  and  $-4.5$  eV. The band at  $-12.7$  eV involves s orbitals of C and H in the methyl group and oxygen p orbitals.

#### 4. Partially Hydroxylated Surface

On the basis of SFG measurements, it has been recently proposed that surface methoxy groups on anatase are the products of the reaction between  $\text{CH}_3\text{OH}$  and surface hydroxyls,<sup>8</sup> with the latter formed by water dissociation at vacancies.<sup>9,18,19</sup> As oxygen vacancies are generated by UV irradiation, the overall process results in increased SFG signal from methoxy after UV pretreatment of the sample.

In this section we try to make contact with this experimental work by studying the interaction of methanol with a partially hydroxylated anatase(101) surface, which has two bridging hydroxyl groups ideally generated by dissociation of a  $\text{H}_2\text{O}$  molecule at a vacancy.<sup>18</sup> We start by considering the energetics of the reaction depicted in Scheme 1, where a  $\text{CH}_3\text{OH}$  molecule displaces a  $\text{H}_2\text{O}$  molecule.<sup>8,26</sup> In the product  $\text{TiOCH}_3$  a bridging methoxy replaces a bridging OH ( $\text{OH}_b$ ), which is removed as

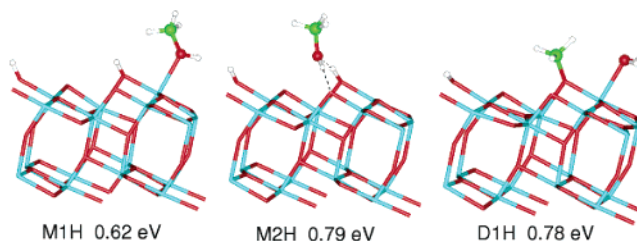


**Figure 8.** Optimized adsorption structures and energies (relative to noninteracting  $\text{CH}_3\text{OH}$  molecule and hydroxylated slab) for methanol molecular and dissociative adsorption on partially hydroxylated surface.

molecular water. We have optimized the initial ( $\text{TiOH}$ ) and final ( $\text{TiOCH}_3$ ) structures, and found that the reaction in Scheme 1 is essentially thermoneutral. At variance with the clean surface, the final state, with a bridging methoxy and a bridging OH, is found to be stable in a 2.5 ps MD trajectory at 160 K. Thus, the thermodynamic driving force of the water displacement reaction could be the subsequent binding of water to a  $\text{Ti}_{5c}$ , which releases 0.6–0.7 eV.<sup>16,21</sup>

To obtain some hints on the reaction mechanisms, we carried out two MD simulations: in one case we placed a  $\text{CH}_3\text{OH}$  above an  $\text{OH}_b$  and in the other case  $\text{CH}_3\text{OH}$  was adsorbed to a  $\text{Ti}_{5c}$  close to the  $\text{OH}_b$ . In both trajectories the molecule moved to a new coordination mode, where its hydroxyl accepts a hydrogen bond from the  $\text{OH}_b$  and donates one Hb to another  $\text{OH}_b$  (M2H, Figure 8). This state, bridging between two  $\text{O}_{2c}$ , appears to be very stable: indeed, after geometry optimization, it turns out to be 0.17 eV more stable than the state with  $\text{CH}_3\text{OH}$  adsorbed on a  $\text{Ti}_{5c}$  (M1H in Figure 8). It is roughly isoenergetic with the dissociated state D1H, where the formed  $\text{H}_2\text{O}$  molecule binds to the same  $\text{Ti}_{5c}$  as the methoxy group. These results suggest that the first step of methanol dissociation on the hydroxylated surface is likely to be the formation of state M2H, which cannot be formed on the nonhydroxylated surface. This state was formed in MD trajectories of either a single methanol or a full monolayer on the hydroxylated surface. However, no actual dissociation was observed in a 4–5 ps MD run, even after increasing the temperature to 300 K. This suggests the presence of an energy barrier between states M2H and D1H, which hinders dissociation on the relatively short time scale accessible to our simulations. Moreover, the overall reaction is likely to involve several intermediate states.<sup>26</sup> Interestingly, state M1H was occasionally reformed during the 300 K MD run, so that the possibility of a direct  $\text{M1H} \rightarrow \text{D1H}$  conversion cannot be ruled out.

#### 5. Conclusions

Several new results have emerged from the present calculations, providing further structural and dynamic details to the existing picture of methanol adsorption on  $\text{TiO}_2$  surfaces.

In agreement with experiment, our results show that molecular adsorption is thermodynamically favored on the anatase surface, unless defects or surface hydroxyls are present. However, due to the low density of oxygen vacancies on anatase,<sup>7</sup> the reaction with surface hydroxyls may be more relevant for the formation of methoxy groups.

Two molecular adsorption modes are found to coexist in a methanol monolayer. This is at variance with water adsorption, where a flat monolayer with a uniform adsorption mode is formed.<sup>21</sup> The two adsorption modes for a methanol monolayer give rise to specific features in the high-frequency vibrational bands and in the electronic density of states. The latter shows methanol-induced states close to the top of the O-2p valence

band, which explains the role of methanol as a hole scavenger in photocatalysis.

Our molecular dynamics simulations suggest that the reaction of methanol with surface hydroxyls involves at least one intermediate state: the first step of the process is likely the formation of a new molecular adsorption state, which is not stable on the clean surface. However, further work is needed to study the mechanism of this process.

**Acknowledgment.** This work was supported by the National Science Foundation under Grant No. CHE-0121432. The calculations were performed on the Lemieux Terascale Computing System at the Pittsburgh Supercomputer Center, the IBM SP3 at the Keck Computational Materials Science Laboratory in Princeton, and the Cadillac cluster at the Princeton Institute for Computational Science and Engineering.

## References and Notes

- (1) Diebold, U. *Surf. Sci. Rep.* **2002**, *293*, 1.
- (2) Hoffmann, M. R.; Martin, S. T.; Choi, W.; Bahnemann, D. W. *Chem. Rev.* **1995**, *95*, 69–96.
- (3) Henderson, M. A.; Otero-Tapia, S.; Castro, M. E. *Faraday Discuss.* **1999**, *114*, 313.
- (4) Kim, S.; Choi, W. *J. Phys. Chem. B* **2002**, *106*, 13311.
- (5) Morand, R.; Lopez, C.; Koudelka-Hep, M.; Kedzierzawski, P.; Augustynski, J. *J. Phys. Chem. B* **2002**, *106*, 7218.
- (6) Bates, S. P.; Gillan, M. J.; Kresse, G. *J. Phys. Chem. B* **1998**, *102*, 2017.
- (7) Herman, G. S.; Dohnalek, Z.; Ruzyski, N.; Diebold, U. *J. Phys. Chem. B* **2003**, *107*, 2788.
- (8) Wang, C.; Groenzin, H.; Shultz, M. J. *J. Phys. Chem. B* **2003**, *108*, 265.
- (9) Schaub, R.; Thorstrup, P.; Laegsgaard, E.; Steensgaard, I.; Norskov, J. K.; Besenbacher, F. *Phys. Rev. Lett.* **2001**, *87*, 266104.
- (10) The possibility of water dissociation at nondefect sites on TiO<sub>2</sub>-(110) has been controversial for many years, see, e.g.: Henderson, M. A. *Surf. Sci. Rep.* **2002**, *46*, 1. However, recent experiments (ref 9) and calculations (Harris, L. A.; Quong, A. A. *Phys. Rev. Lett.* **2004**, *93*, 086105) appear to indicate preferential molecular adsorption on the ideal surface at coverages up to 1 ML.
- (11) Kavan, L.; Grätzel, M.; Gilbert, S. E.; Klemenz, C.; Scheel, H. J. *J. Am. Chem. Soc.* **1996**, *118*, 6716.
- (12) Car, R.; Parrinello, M. *Phys. Rev. Lett.* **1985**, *55*, 2471.
- (13) Perdew, J. P.; Burke, K.; Ernzerhof, M. *Phys. Rev. Lett.* **1996**, *77*, 3865.
- (14) Vanderbilt, D. *Phys. Rev. B* **1990**, *41*, 7892.
- (15) Lazzeri, M.; Vittadini, A.; Selloni, A. *Phys. Rev. B* **2001**, *63*, 155409.
- (16) Vittadini, A.; Selloni, A.; Rotzinger, F. P.; Grätzel, M. *Phys. Rev. Lett.* **1998**, *81*, 2954.
- (17) Vittadini, A.; Selloni, A.; Rotzinger, F. P.; Grätzel, M. *J. Phys. Chem. B* **2000**, *104*, 1300–1306.
- (18) Tilocca, A.; Selloni, A. *J. Chem. Phys.* **2003**, *119*, 7445.
- (19) Tilocca, A.; Selloni, A. *J. Phys. Chem. B* **2004**, *8*, 4743.
- (20) Nosè, S. *Mol. Phys.* **1984**, *52*, 255.
- (21) Tilocca, A.; Selloni, A. *Langmuir* **2004**, *20*, 8379.
- (22) Lide, D. *CRC Handbook of Chemistry and Physics*, 84th ed.; CRC Press: Boca Raton, FL, 2004.
- (23) Blanksby, S. J.; Ellison, G. B. *Acc. Chem. Res.* **2003**, *36*, 255.
- (24) Langel, W. *Surf. Sci.* **2002**, *496*, 141–150.
- (25) Lindan, P. J. D.; Harrison, N. M.; Gillan, M. J. *Phys. Rev. Lett.* **1998**, *80*, 762–765.
- (26) Wang, C.; Groenzin, H.; Shultz, M. J. *J. Am. Chem. Soc.* **2004**, *126*, 8094.
- (27) Wu, W.-C.; Chuang, C.-C.; Lin, J.-L. *J. Phys. Chem. B* **2000**, *104*, 8719.